Numerical Simulation of Multiphase Flow in Nanoporous Organic Matter With Application to Coal and Gas Shale Systems

AGU PUBLICATIONS

Water Resources Research

RESEARCH ARTICLE
10.1002/2017WR021500

Key Points:
- A multiphase pore network flow model is proposed to study gas-water flow pattern in nanoporous organic matter
- Effects of slip length, contact angle, flow area on water flow are considered and gas flow accounts for full range of transport mechanisms
- Water relative permeabilities decrease and gas relative permeabilities increase with the decrease of pore size

Supporting Information:
- Supporting Information S1

Correspondence to:
J. Yao,
rcogfr_upc@126.com

Citation:
Song, W., Yao, J., Ma, J., Sun, H., Li, Y., Yang, Y., & Zhang, L. (2018). Numerical simulation of multiphase flow in nanoporous organic matter with application to coal and gas shale systems. *Water Resources Research*, *54*, 1077–1092. https://doi.org/10.1002/2017WR021500

Received 12 JUL 2017
Accepted 2 FEB 2018
Accepted article online 8 FEB 2018
Published online 20 FEB 2018

Numerical Simulation of Multiphase Flow in Nanoporous Organic Matter With Application to Coal and Gas Shale Systems

Wenhui Song[1], Jun Yao[1], Jingsheng Ma[2], Hai Sun[1], Yang Li[3], Yongfei Yang[1], and Lei Zhang[1]

[1]Research Centre of Multiphase Flow in Porous Media, China University of Petroleum (East China), Huangdao District, Qingdao, China, [2]School of Energy, Geoscience, Infrastructure and Society, Heriot-Watt University, Edinburgh, UK, [3]Department of Oilfield Exploration and Development, Sinopec, Beijing, China

Abstract Fluid flow in nanoscale organic pores is known to be affected by fluid transport mechanisms and properties within confined pore space. The flow of gas and water shows notably different characteristics compared with conventional continuum modeling approach. A pore network flow model is developed and implemented in this work. A 3-D organic pore network model is constructed from 3-D image that is reconstructed from 2-D shale SEM image of organic-rich sample. The 3-D pore network model is assumed to be gas-wet and to contain initially gas-filled pores only, and the flow model is concerned with drainage process. Gas flow considers a full range of gas transport mechanisms, including viscous flow, Knudsen diffusion, surface diffusion, ad/desorption, and gas PVT and viscosity using a modified van der Waals' EoS and a correlation for natural gas, respectively. The influences of slip length, contact angle, and gas adsorption layer on water flow are considered. Surface tension considers the pore size and temperature effects. Invasion percolation is applied to calculate gas-water relative permeability. The results indicate that the influences of pore pressure and temperature on water phase relative permeabilities are negligible while gas phase relative permeabilities are relatively larger in higher temperatures and lower pore pressures. Gas phase relative permeability increases while water phase relative permeability decreases with the shrinkage of pore size. This can be attributed to the fact that gas adsorption layer decreases the effective flow area of the water phase and surface diffusion capacity for adsorbed gas is enhanced in small pore size.

1. Introduction

Coal and gas shales are complex systems that contain carbon-based 3-D pore networks with a significant amount of surface area contained in the nanoscale pores (Chalmers et al., 2012; Nelson, 2009; Wu et al., 2017). Since the size of coal and shale pores approaches to the molecular mean free path, gas flows deviate from pure viscous flow due to nanoconfinement effects. Knudsen number is defined as the ratio of molecular mean free path to the pore radius and is conventionally used to demarcate the flow regimes (Civan, 2010; Loyalka & Hamoodi, 1990). It is well known that in an organic-rich pores, in particular, a large amount of methane molecules may be adsorbed onto pore surfaces under physical sorption. This gives rise to two phenomena (Song et al., 2016a; Sun et al., 2015): the adsorbed gas molecules reduce pore space available for nonadsorbed or free gas molecules to flow, while the surface diffusion may take place within the adsorbed gas to enhance the transport of gas molecules along molecular concentration gradients. These phenomena become relatively more important in nanoscale pores and must be considered in full. It has been shown (Akkutlu & Didar, 2013; Devegowda et al., 2012; Islam et al., 2015a) that in confined porous space the critical pressure (P_c) and temperature (T_c) of natural gas depend on the size of pores and therefore such effect must be accounted for in an Equation of State (EoS) and determination of in situ properties of the gas of concern. Two types of gas flow models at confined pore space have been developed. Beskok and Karniadakis (1999) developed a unified Hagen-Poiseuille-type model covering the fundamental flow regimes in tight porous media, including continuum fluid flow, slip flow, transition flow, and free molecular flow conditions. This model has been adopted and expanded by Civan (2010) and Civan et al. (2011, 2013) to consider the effect of the characteristic parameters of porous media and by Xiong et al. (2012) to model surface diffusion of adsorbed gas, which is of crucial importance in organic pores. Another type of models is based on superposing slip flow and Knudsen diffusion on the top the Darcy (Darabi et al., 2012; Ghanbarian

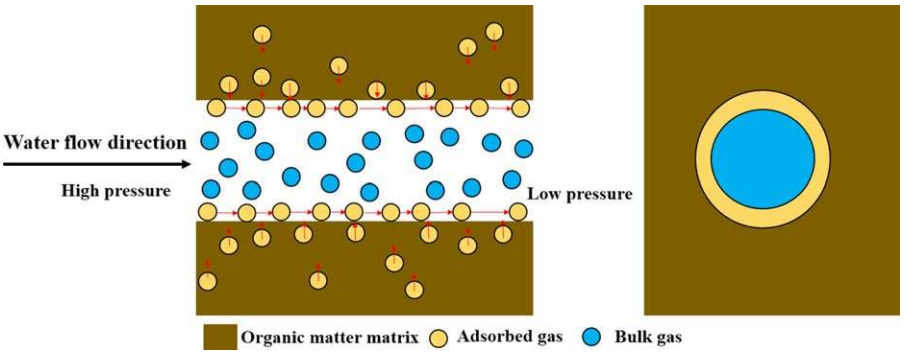

Figure 1. Illustration of gas flow in nanoscale organic pores (adsorbed gas flows on the pore surface via surface diffusion while bulk gas flows in the center of the pore by viscous flow and Knudsen diffusion).

& Javadpour, 2017; Javadpour, 2009; Javadpour et al., 2007; Singh, 2013; Singh & Javadpour, 2016) in a linear fashion. Wu et al. (2014) showed for such models appropriate weighting coefficients may be determined via probabilities between gas molecules colliding with each other and colliding with nanopores wall to elaborate the relative importance among non-Darcy flow effects given a gas flow condition.

The assumption of nonslip flow boundary conditions at the inner pore walls underestimates water flow in the nanoporous organic matter (Belyaev & Vinogradova, 2010; Lauga & Stone, 2003; Neto et al., 2005; Vinogradova, 1999). The structural and dynamical properties of confined water in nanopores are notably different from bulk water (Liu et al., 2005; Mashl et al., 2003). The viscosity of confined water in nanopores changes significantly (Campbell et al., 1996; Gao et al., 2007; Goertz et al., 2007) and the no-slip boundary condition is not valid (Cottin-Bizonne et al., 2003; Holt et al., 2006; Majumder et al., 2005), which can be attributed to relative strength of the water-wall interaction and the water intermolecular interaction (Cottin-Bizonne et al., 2003; Granick et al., 2003). Barrat and Bocquet (1999) showed that at large enough contact angle, the boundary condition can be drastically different from a no-slip condition. Holt et al. (2006) and Majumder et al. (2005) found that the flow rates for water flow through membranes of carbon nanotubes (CNTs) with diameters of 1.3–7.0 nm, are 2–5 orders of magnitude greater than those calculated by the no-slip Hagen-Poiseuille equation. The flow rate of water through 44 nm carbon nanopipes measured by Whitby et al. (2008) is an order of magnitude greater than the no-slip Hagen-Poiseuille equation. Vinogradova (1995) suggested that the slippage is linked to the decrease in viscosity of the thin layer near the wall. Javadpour et al. (2015) measured slip length of brine and pores in shale by using an atomic force microscope (AFM). Wu et al. (2017) considered the influence of the wettability, viscosity, and nanopore dimension on confined water flow and proposed a simple model based on the modified Hagen-Poiseuille equation. Berg et al. (2007) experiment indicates that the endpoint relative permeabilities larger than one for two phase flow in porous rock can be attributed to the slip boundary condition.

Modeling fluid flow in resolved pore space of nanoporous material has benefited from the recent advancement in high-resolution imaging and development of pore characterization techniques (Chen et al., 2015a,

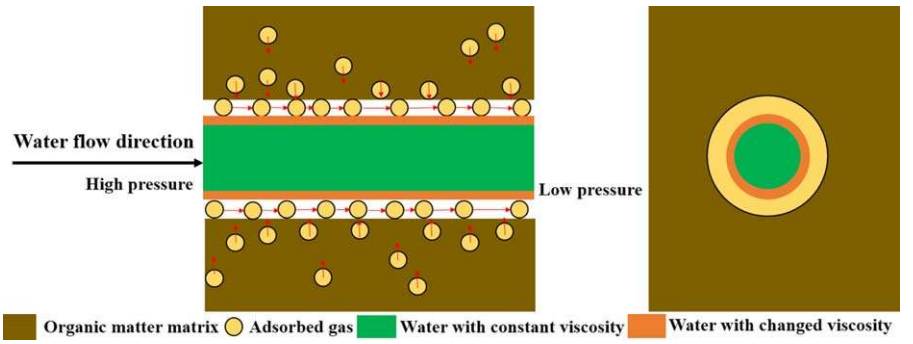

Figure 2. Illustration of water and adsorbed gas flow after the bulk gas is displaced by water in nanoscale organic pores (adsorbed gas flows on the pore surface via surface diffusion while water flows in the center of the pore influenced by slip length and contact angle). The adsorbed gas can be deemed as gas film at the boundary of the pore wall.

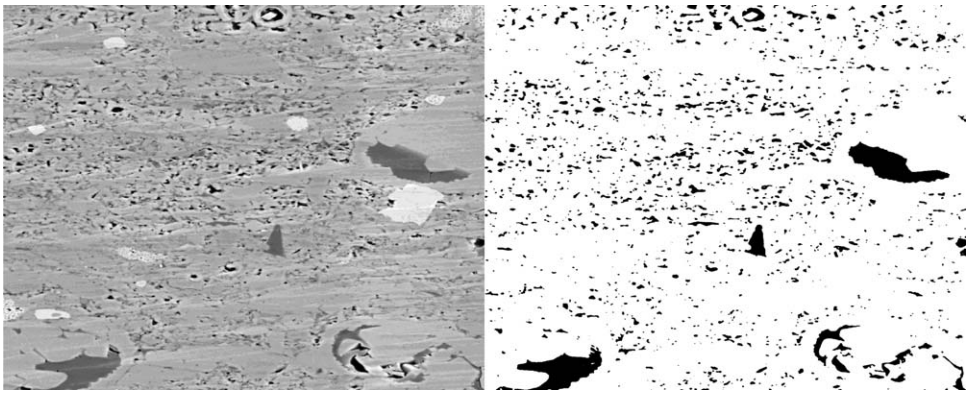

Figure 3. A section of a shale SEM image of a 2-D polished thin section (Walls & Sinclair, 2011): (a) unsegmented and (b) segmented. The section is about 18.3 μm × 14.6 μm at a pixel size of 12 nm × 12 nm.

2015b, 2015c; Dewers et al., 2012; Song et al., 2016b; Suhrer et al., 2013). This has led to the development of simplified representation of a complex pore space as a realistic pore network of connected pore nodes and throats, to enable efficient simulation of fluid flow (Dong & Blunt, 2009; Yi et al., 2017). Most pore network models reported account for a subset of the flow regimes for single phase fluid flow only (Afsharpoor & Javadpour, 2016; Huang et al., 2016; Mehmani et al., 2013; Zhang et al., 2015). In our previous work, we developed a pore network flow model capable of simulating nonideal gas flow (Ma & Couples, 2015; Ma et al., 2014a, 2014b) and that model was expanded further to consider the effect of adsorbed layers on the free gas flow with modeling the surface diffusion (Song et al., 2017). The objective of this work is to develop a pore network flow model for nanoporous organic matter to investigate the multiphase flow pattern. Gas flow considers a full range of gas transport mechanisms, including viscous flow, slip flow, Knudsen diffusion, surface diffusion, ad/desorption in nanoscale pores, and gas PVT and viscosity using a modified van der Waals' EoS and a correlation for natural gas, respectively. The influences of slip length, contact angle, and gas adsorption layer on water flow are considered. Surface tension considers the pore size and temperature effects. Invasion percolation is applied to calculate gas-water relative permeability and the influences of pore pressure, temperature, and pore size on gas-water relative permeability are investigated. To the best knowledge of the author, this is the first study on analyzing multiphase flow behaviors in nanoscale organic porous media by considering such a variable sets of gas transport mechanisms.

This paper is organized as follows. In section 2, gas and water flow conductances for a cylindrical capillary are formulated. Gas flow conductance considers the influences of gas transport mechanisms, gas adsorption/

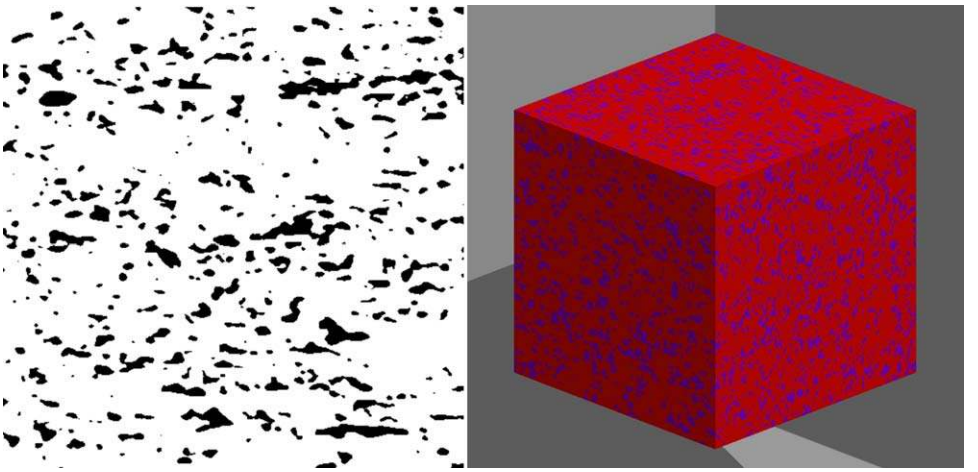

Figure 4. (a) Selected binary subsection used for 3-D reconstruction (400 × 400 pixels). (b) Reconstructed 3-D model (red represents matrix blue represents pore space). The image contains 400 × 400 × 400 voxels at a voxel size of 12 nm and depicts about 4.8 μm cube.

desorption, real gas PVT, and T_c, P_c change. Water flow conductance considers slip length, contact angle, and gas adsorption layer. Section 3 applies the proposed two phase pore network flow model to a realistic organic pore network of a reconstructed 3-D model from 2-D section of a gas shale sample. The solution method is introduced and result is given. Detailed analysis is conducted in section 4. This is followed by a section comprising major conclusion.

2. Fluid Flow Model for a Cylindrical Capillary

The gas flow conductance developed in this section takes into consideration the following effects: (1) gas flow in the full range of gas flow regimes; (2) gas sorption, (3) pore-surface diffusion, and (4) gas PVT and viscosity. Detailed derivations are given in Appendix A. Xu and Dehghanpour (2014), Lan et al. (2015), and Li et al. (2016, 2017) suggested that the surface of the organic matter is gas-wet. Molecular simulation results indicate that for organic carbon material with hydrophobic pore surface, adsorbed methane molecules occupy pore surface and water molecules locate at the center of the pore (Lee et al., 2016). Because currently two phase flow experiment and methane-water molecular simulation data based on realistic organic matter (kerogen) model are not available, therefore we assumes that once water flows into the nanopore under certain pressure drop, the bulk gas is displaced and water flows in the center of the pore while adsorbed gas flows at the boundary of pore in the forms of surface diffusion. This assumption is valid in physical sense because adsorbed gas constantly desorbs from inner organic matrix to the pore wall and our model can be viewed as the conceptual model to study gas-water flow pattern in nanoscale organic matter under reasonable assumption mentioned above. The adsorbed gas flow conductance is given in equation (A29). It has been proved by experiments (Ortiz-Young et al., 2013; Raviv et al., 2001) and molecular simulation results (Hoang & Galliero, 2012; Neek-Amal et al., 2016; Thomas & McGaughey, 2008) that the viscosity of confined water changes at the boundary of a pore within a zone of a certain thickness T_{wat}. Based on Wu et al. (2017), the thickness of the viscosity varying zone T_{wat} can be determined as 0.7 nm and the changed viscosity is the function of a contact angle, which can be written as equation (1). Detailed explanations are given in Figures 1 and 2.

$$\frac{\mu_i}{\mu_\infty} = -0.018\theta_w + 3.25 \tag{1}$$

where μ_i is the changed water viscosity (Pa·s), μ_∞ is the constant water viscosity as a function of temperature (Pa·s), and θ_w is the water contact angle.

The effective flow radius r_{eff_water} for water in consideration of adsorbed gas film can be written as

$$r_{eff\_water} = r - d_m\theta \tag{2}$$

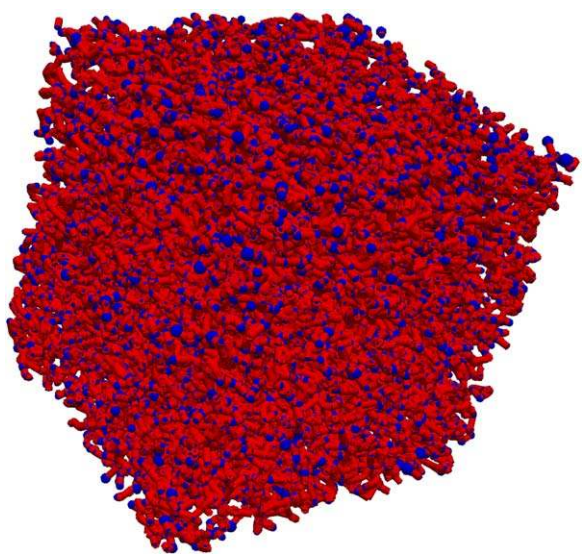

Figure 5. Extracted organic pore network (red represents throats blue represents pores).

where r is the pore radius (m), d_m is the gas molecular diameter (m), and θ is gas coverage of real gas, dimensionless. The effective viscosity of the confined water $\mu(r_{eff\_water})$ is calculated by area weighted average of the changed viscosity and constant viscosity in nanopores (Thomas & McGaughey, 2008):

$$\mu(r_{eff\_water}) = \mu_i \frac{A_i(r_{eff\_water} - T_{wat})}{A_t(r_{eff\_water})} + \mu_\infty \left[1 - \frac{A_i(r_{eff\_water} - T_{wat})}{A_t(r_{eff\_water})}\right] \tag{3}$$

where A_i is the water flow area with constant viscosity for a single pore (m^2) and A_t is water flow total area for a single pore (m^2). The constant water viscosity as a function of temperature T is given in equation (4) and viscosity of water $\mu_\infty(T)$ can be predicted with accuracy to within 2.5% from 273 to 643 K (Al-Shemmeri, 2012):

$$\mu_\infty(T) = 2.414 \times 10^{-5} \times 10^{247.8/(T-140)} \tag{4}$$

Because the surface of organic matter is deemed as gas-wet, the water and adsorbed gas interface can be regarded as the hydrophobic pore surface for water flow. For hydrophobic pore surface, Wu et al. (2017) derived a scaling function for the slip length based on the

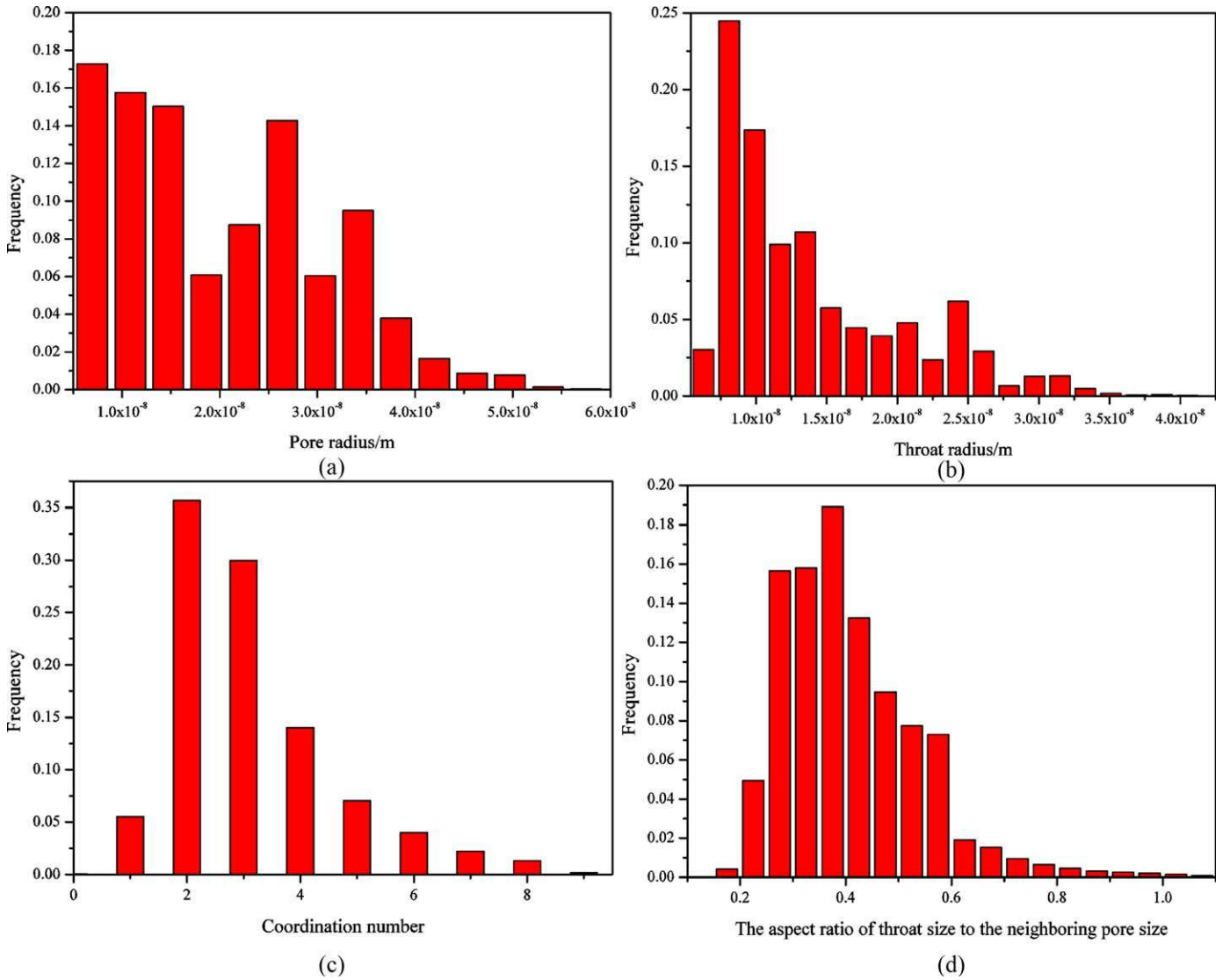

Figure 6. Pore network structure characteristics: (a) pore-size distribution, (b) throat-size distribution, (c) coordination number distribution, and (d) distribution of the aspect ratio of throat size to the neighboring pore size.

published MD simulation data shown in equation (5) and the confined water flow rate Q_{water} is given in equation (6).

$$l_{st} = \frac{0.41}{(\cos\theta_w + 1)^2} \tag{5}$$

$$Q_{water} = \frac{\pi}{8\mu(r_{eff\_water})}\left[r^4_{eff\_water} + 4r^3_{eff\_water}l_{st}\right]\frac{dp}{dx} \tag{6}$$

where l_{st} is the water slip length in a single pore (m) and p is the pore pressure (Pa). Therefore, water flow conductance g_{water} can be written as

$$g_{water} = \frac{\pi}{8\mu(r_{eff\_water})l}\left[r^4_{eff\_water} + 4r^3_{eff\_water}l_{st}\right] \tag{7}$$

Based on experiment and molecular simulation data, the water surface tension γ_{w0} change versus temperature T can be given as (Vega & De Miguel, 2007)

Table 1
Basic Simulation Parameters Used for Multiphase Quasi-Static Pore Network Flow Model

Reservoir properties	
Formation temperature T (K)	400
Pore pressure p (MPa)	40
Pressure gradient dp/dx (MPa/m)	0.1
Total organic grain volume per total grain volume ε_{ks}	0.01 (Wasaki & Akkutlu, 2015)
Water contact angle θ_w (°)	103
Gas properties	
Langmuir pressure p_L (MPa)	13.789514 (Wasaki & Akkutlu, 2015)
Maximum adsorbed gas concentration C_{max} (mol/m^3)	328.7 (Wasaki & Akkutlu, 2015)
Isosteric adsorption heat at zero gas coverage $\Delta H(0)$ (J/mol)	16,000 (Wu et al., 2015)
Fitting coefficients of isosteric adsorption heat γ (J/mol)	−4,186 (Wu et al., 2015)
Ideal gas constant R (J/(mol k))	8.314
Ratio of the rate constant for blockage to the rate constant for forward migration κ	0.5 (Wu et al., 2016)
Molecular weight M (kg/mol)	0.016
Parameters used in determining phase change taken from (Islam et al., 2015b)	
vdW energy parameter a (m^6 Pa/mol^2)	0.22998
vdW energy parameter b (m^3/mol)	4.28×10^{-5}
Lennard-Jones size parameter σ (m)	3.73×10^{-9}
Lennard-Jones energy parameter ε	2.0434×10^{-21}

$$\gamma_{w0}=227.86(1-T/T_{c\_water})^{11/9}(1-0.6413(1-T/T_{c\_water}))\times 10^{-3} \tag{8}$$

where T_{c_water} is the critical temperature for water, 641.4 K. The dependence of surface tension γ_w on water curvature radius r_c is given in equations (9) and (10) (Lu & Jiang, 2005) and curvature radius r_c is related with effective flow radius r_{eff_water} by equation (11) (Kloubek, 1981).

$$\gamma_w=\gamma_{w0}\left(1-\frac{1}{4r_c/h-1}\right)\exp\left(-\frac{2S_b}{3R}\frac{1}{4r_c/h-1}\right) \tag{9}$$

$$S_b=\frac{E_0}{T_b} \tag{10}$$

$$r_c=-\frac{r_{eff\_water}}{\cos\theta_w} \tag{11}$$

where h is O—H bond length, 0.096 nm, R is the ideal gas constant, 8.314 J/(K mol), S_b is solid-vapor transition entropy of water, E_0 is the bulk solid-vapor transition enthalpy (J/mol), T_b is bulk solid-vapor transition temperature of water (K), and θ_w is the water contact angle.

3. Construction of Multiphase Flow Model for 3-D Pore Networks

3.1. Construction of a 3-D Organic Matter Model and Pore Network Model

A section of a high-resolution SEM image of an organic matter-rich gas shale sample is applied in this work (Walls & Sinclair, 2011; Figure 3). More detailed image information can be seen in the Supporting Information S1. The resolution of the SEM image is 1,526 × 1,220 pixels and the pixel size of the SEM image taken is 12 nm × 12 nm. The grey-scale subsection image was first segmented into pore phase and matrix by applying a median filter and then Otsu segmentation (Jassim & Altaani, 2013). Then a binary subsection about 400 × 400 pixels was used and a 3-D binary model was reconstructed in Figure 4 using the Multiple-Point Statistics (MPS) method (Okabe & Blunt, 2005) following the same procedure described in (Yang et al., 2015). The resulting 3-D model contains 400 × 400 × 400 voxels at a voxel size of about 12 nm. Then the maximal ball fitting method (Blunt et al., 2013; Dong & Blunt, 2009) was applied to extract its pore network. The organic pore network extracted is shown in Figure 5. Expressed in terms of hydraulic radius, the pore-size and throat-size distributions are shown in Figures 6a and 6b, respectively. The average coordination number in Figure 6c is 3 and is smaller than the typical coordination number for sandstone (Arns et al., 2004; Lindquist et al., 2000). A 40% of the total pores are poorly connected (coordination number equals to 0 or 1) and dead-end pores occupy 5% of the total pores. The average aspect ratio of throat size to the

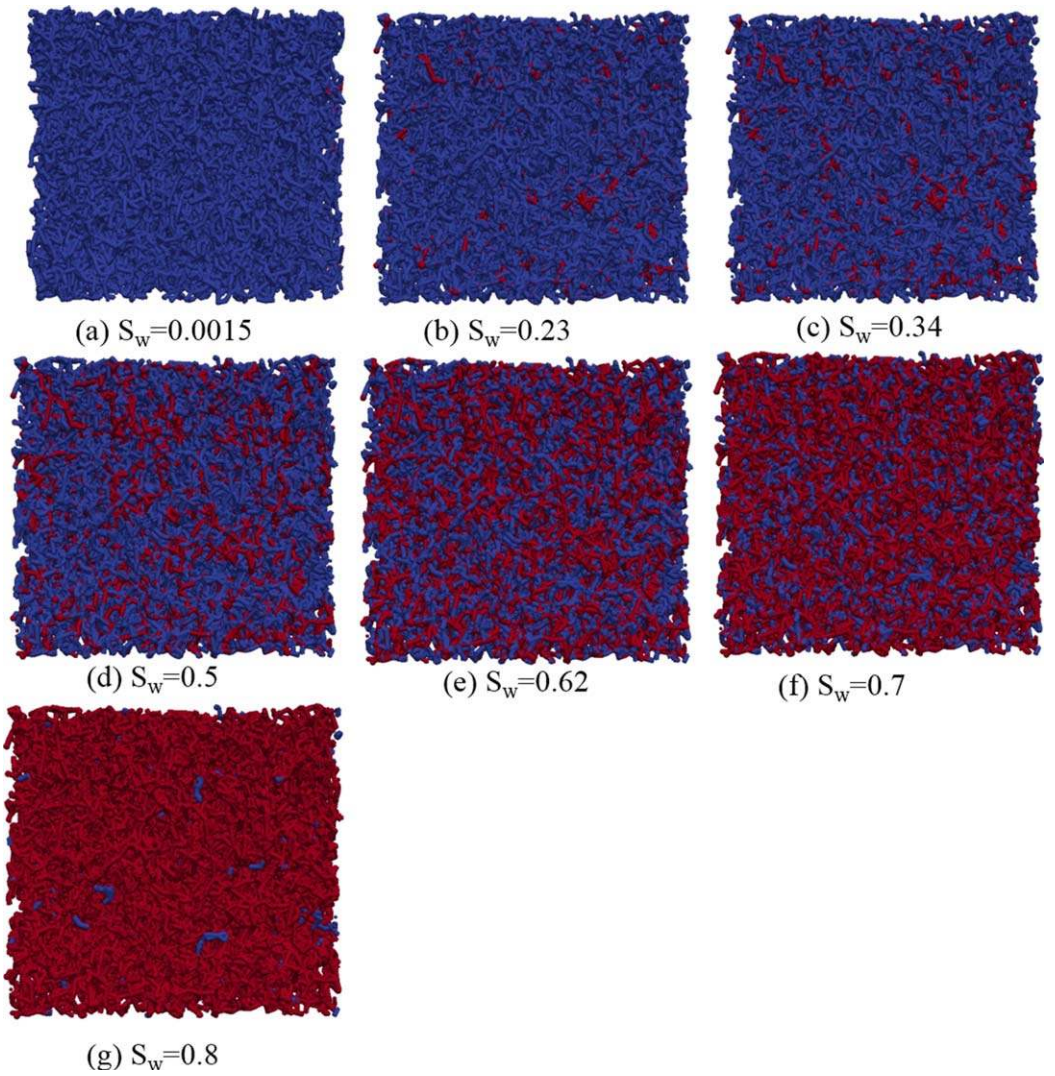

Figure 7. Visualization of gas and water distribution during drainage process, the water is injected from the right side (red color represents water, blue color represents bulk gas, the residual gas saturation S_g is 0.2, shown in (g)). (a) S_w = 0.0015, (b) S_w = 0.23, (c) S_w = 0.34, (d) S_w = 0.5, (e) S_w = 0.62, (f) S_w = 0.7, and (g) S_w = 0.8.

neighbouring pore size in Figure 6d is 0.41 and is similar to the average aspect ratio for the sandstone (Arns et al., 2003). Note that although not all of the imaged pores are organic in this actual sample, they are treated as if they are in this work.

3.2. Multiphase Quasi-Static Pore Network Flow Model

The organic pores forming during hydrocarbon accumulation and generation processes are generally hydrophobic and almost without water (Odusina et al., 2011). Korb et al. (2014) found that the initial water mainly stores in inorganic pores. Li et al. (2017) showed that the storage of water inside organic pores can be neglected. Initially, the network is fully saturated with free gas and adsorbed gas and is strongly gas-wet. Therefore, the irreducible water saturation inside the nanoporous organic matter is zero. Then, water enters the network representing migration into the reservoir. At every stage of the process, water invades the available pore body or throat with the entry capillary pressure. This forms the basis for the invasion percolation algorithm used previously (Chandler et al., 1982; Oren et al., 1998; Valvatne, 2004; Wilkinson & Willemsen, 1983) to model drainage processes. In this study, the pore shape is simplified as the circular shape and the hydraulic radius can be expressed as equation (12) as done in Oren et al. (1998), Valvatne and Blunt (2004), and Ma et al. (2014a). The entry capillary pressures P_{cw} for circular pore is given in equation (13) (Valvatne, 2004). The drainage pressure from inlet side starts from lowest capillary pressure to the largest entry

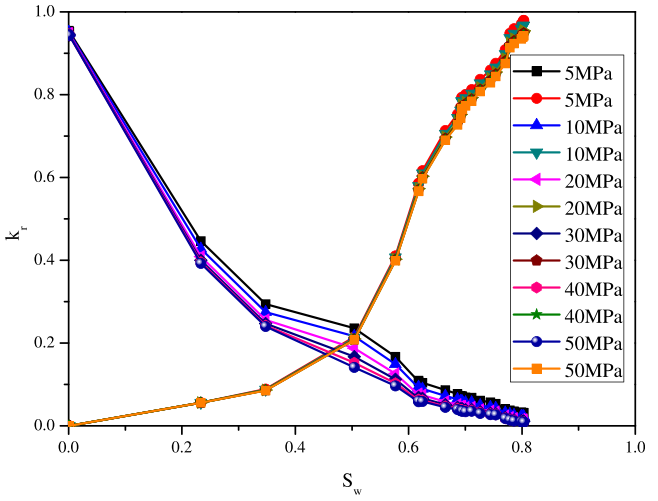

Figure 8. Gas-water relative permeabilities at different pore pressures, $T = 400$ K.

capillary pressure. Detailed model parameters are given in Table 1. The water saturation is obtained by dividing the total volume of invaded pores occupied by water by the total pore volume. Visualization of gas and water distribution during drainage process is shown in Figure 7.

$$r = \frac{2A}{P_d} = 2\sqrt{AG} \tag{12}$$

$$P_{cw} = \frac{2\gamma_w \cos\theta_w}{r_{eff\_or}} \tag{13}$$

where A is the area of pore cross section (m^2), P_d is the perimeter of the pore cross section (m), and G is shape factor of the pore cross section, dimensionless. Because of the existence of water slip and gas rarefied effect in nanopores, the absolute permeability k_{abs_water} calculated by water is different from the absolute permeability k_{abs_gas} calculated by gas. Therefore, unlike the traditional pore network models, the absolute permeability should be calculated for each phase to obtain the reasonable value of relative permeability. The water phase absolute permeability is obtained by equation (14). Because the viscosity is variable across pores and throats, and pressure-dependent, gas phase absolute permeability is calculated using a different way to that which would be normally done (see Oren et al., 1998) by equation (14). That is, the product of gas flux and viscosity is calculated for every inlet pore voxel to compute the sum of the total flux at the inlet face and gas phase absolute permeability by equation (15).

$$k_{abs\_water} = \frac{\mu L_{pnm} \sum_{i=1}^{N_{inlet}} q_{inlet}}{A_{pnm} \Delta p} \tag{14}$$

$$k_{abs\_gas} = \frac{\sum_{i=1}^{N_{inlet}} q_{inlet} \mu_{inlet} L_{pnm}}{A_{pnm} \Delta p} \tag{15}$$

where q_{inlet} is gas flux in inlet pores (m^3/s), N_{inlet} is the number of the inlet pores, L_{pnm} is the length of the 3-D model, A_{pnm} is area of the 3-D model cross section (m^2), μ_{inlet} is the gas viscosity in inlet pores(Pa·s), and ΔP is the pressure drop on the 3-D model (Pa). The relative permeability is then given by

$$k_{r\_water} = \frac{q_{tmp\_water}}{q_{tsp\_water}} \tag{16}$$

$$k_{r\_gas} = \frac{q_{tmp\_gas}}{q_{tsp\_gas}} \tag{17}$$

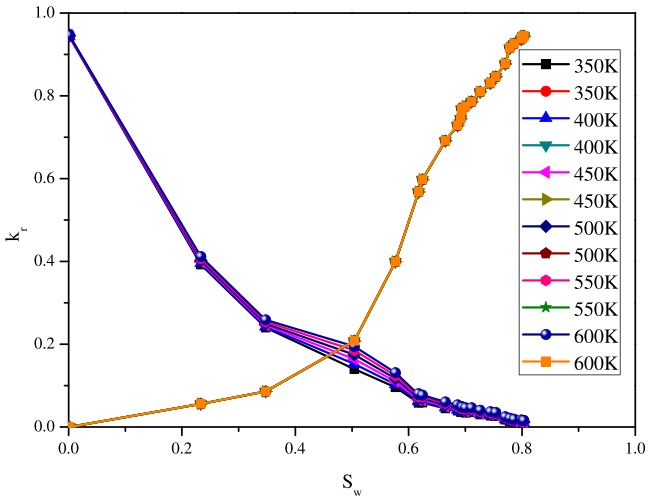

Figure 9. Gas-water relative permeabilities at different temperatures, $P = 40$ MPa.

q_{tmp} is the total flow rate of phase p in multiphase conditions with the same imposed pressure drop. The total flow rate is found by solving for the pressure everywhere, imposing mass conservation at every pore i. The mass balance equations for gas phase are nonlinear functions of gas pressures due to pressure-dependent conductance and viscosity, and they must be solved iteratively. Taking an initial pressure distribution as that for the Darcy flow, the system of equations is solved iteratively in a similar fashion as in Ma et al. (2014a), until the volumetric flux converges.

$$\sum_{j=1}^{N_i} q_{ij} = 0 \tag{18}$$

where j runs over all the throats connected to pore i. The flow rate q_{ij} between two pores i and j is given by

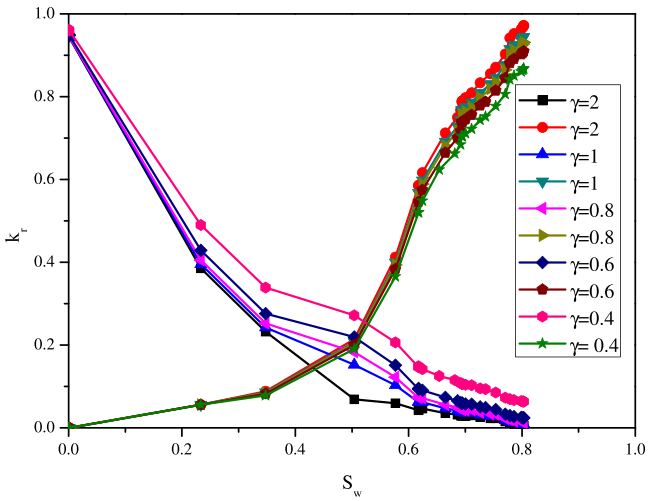

Figure 10. Gas-water relative permeabilities at different pore radius ratio ($P = 40$ MPa, $T = 400$ K).

$$q_{ij} = g_{ij}(p_i - p_j) \tag{19}$$

The conductance between two pore bodies g_{ij} is taken to be the harmonic mean of each individual conductance, as similar done in Valvatne (2004).

$$\frac{L_i + L_t + L_j}{g_{i,j}} = \frac{L_i}{g_i} + \frac{L_t}{g_t} + \frac{L_j}{g_j} \tag{20}$$

where L_i, L_j, and L_t are the length of pore i and pore j and the throat that connects pore i and pore j, respectively (m). g_i, g_j, and g_t are the gas flow conductance of pore i and pore j and the throat that connect pore i and pore j, respectively (m^3/Pa·s).

4. Results and Analysis

Figures 8 and 9 show gas-water relative permeabilities at different pore pressures and temperatures. The influences of pore pressure and temperature on water phase relative permeabilities are negligible while gas phase relative permeabilities are relatively larger in higher temperatures and lower pore pressures. The surface diffusion for adsorbed gas flow after displacement decreases with the increase of the pore pressure, which is caused by the decrease of the reciprocal of the gas density and $d\theta/dp$ in the formulation of the surface diffusion given in equation (A29). The calculated gas flux at certain displacement stage is smaller than that in low pore pressure as a consequence. On the other hand, the influence of temperature and pressure on absolute gas permeability is very small, which is shown in Appendix B. Therefore, gas phase relative permeabilities decrease with the increase of pore pressure. The surface diffusion coefficient in equation (A26) decreases with the increase of temperature and the surface diffusion for adsorbed gas flow after displacement decreases with the increase of the temperature. Therefore, gas phase relative permeabilities decrease with the increase of temperature.

In order to study the influence of pore size on gas-water relative permeabilities, the radius of every pore and throat in the extracted pore network model is rescaled by a factor, γ_i, of 2, 1, 0.8, 0.6, and 0.4 (see equation (21)) to give a numerical average of all throat radii of 31.2, 15.6, 12.48, 9.36, and 6.24 nm, respectively.

$$r_{shrink} = r\gamma_i (i = 1, 2, 3, 4, 5) \tag{21}$$

As a result, all models have the same connectivity and they differ only in terms of their pore radii. Figure 10 shows gas-water relative permeabilities at different pore radius ratio. As the pore size decreases, the ratio of effective water flow area to total flow area δ shown in equation (22) decreases which causes water phase relative permeabilities drop down. The contribution of surface diffusion on gas permeability for single pore at different pore radius is shown in Figure 11. The contribution of surface diffusion on gas permeability is larger in smaller pore sizes than that in larger pore sizes. Therefore, after bulk gas is displaced by water, the adsorbed gas flow capacity enhances and gas phase relative permeabilities increase with the decrease of pore size in Figure 10. It should be noted the basic model assumption is that the process of gas desorption from inner organic matter to organic matter surface exists simultaneously with the gas-water two phase flow process. Therefore, as the water saturation S_w reaches the maximum value 0.803, the gas phase relative permeabilities are not zero when γ_i equals to 0.6 and 0.4. For the conventional gas-wet system, the corresponding water saturation for the relative permeabilities crosspoint should be less than 0.5. In nanoporous organic matter, fluid flow property is highly dependent on pressure, temperature, and pore size. In Figures 8–10, the corresponding water saturation for the relative permeabilities crosspoint can shift to the value

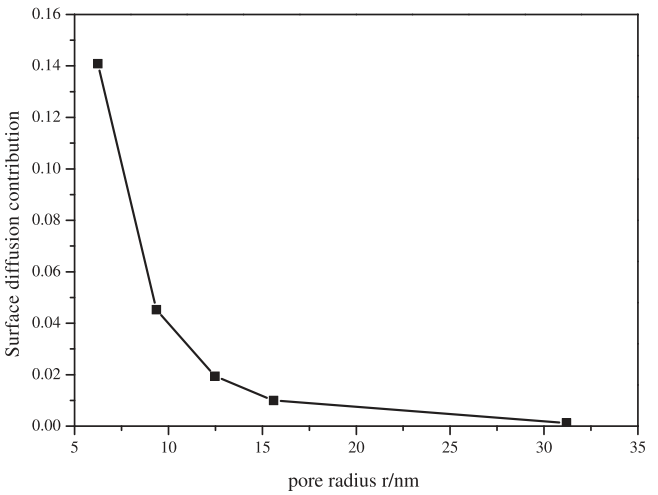

Figure 11. Contribution of surface diffusion on gas permeability for single pore at different pore radius.

larger than 0.5 when pore pressure and average pore radii are lower than 10 MPa and 9.36 nm, respectively, and temperature is larger than 550 K. The fluid distribution in a single pore is influenced by the pore geometry (Arns et al., 2003; Blunt et al., 2002) and numerous pore network models predict multiphase flow pattern based on the corner geometry (Afsharpoor et al., 2017; Hoogland et al., 2016a, 2016b; Joekar-Niasar et al., 2010; Ryazanov et al., 2009; Valvatne & Blunt, 2004). However, the aim of this study is to understand the major effect of the multiphase flow pattern change in various condition. More accurate nanoscale pore network flow model accounting for irregular pore geometry will be considered in the future work.

$$\delta = \frac{A(r_{eff\_water})}{A(r)} = \left(\frac{1 - d_m\theta}{r}\right)^2 \tag{22}$$

5. Conclusion

A multiphase pore network flow model is proposed to study gas-water flow pattern in nanoporous organic matter. Gas flow considers a full range of gas transport mechanisms, including viscous flow, Knudsen diffusion, surface diffusion, ad/desorption in nanoscale pores, and gas PVT and viscosity using a modified van der Waals' EoS and a correlation for natural gas, respectively. The influences of slip length, contact angle, and gas adsorption layer on water flow are considered. Surface tension considers the pore size and temperature effects. Invasion percolation is applied to calculate gas-water relative permeability and the influences of pore pressure, temperature, and pore size on gas-water relative permeability are investigated. The main conclusions are listed as follows:

1. The influences of pore pressure and temperature on water phase relative permeabilities are negligible while gas phase relative permeabilities are relatively larger in higher temperatures and lower pore pressures.
2. Water phase relative permeabilities decrease and gas phase relative permeabilities increase with the decrease of pore size.
3. The corresponding water saturation for the relative permeabilities crosspoint can shift to the value larger than 0.5 in relatively low pore pressure, high temperature and small pore sizes.

Appendix A: Gas Flow Conductance for a Cylindrical Capillary

The gas flow conductance to be developed in this section takes into consideration the following effects: (1) gas flow in the full range of gas flow regimes, (2) gas sorption, (3) pore-surface diffusion, and (4) gas PVT and viscosity. In order to show and model the interwoven nature among these effects in their totality, we formulise the gas flow conductance in the order described below.

A1. Adsorption/Desorption on Capillary and Effective Radius

There are a number of models that may be used to characterise the shale gas adsorptions in different ranges of pressures and temperatures (Charoensuppanimit et al., 2016; Tang et al., 2016; Wang et al., 2016; Yu et al., 2016). At typical shale gas reservoir conditions, there is a consensus from many laboratory studies (Heller & Zoback, 2014) that the Langmuir monolayer adsorption model can adequately capture shale gas adsorption behaviours. For this reason, this model is chosen in this work. This model defines the coverages of a single layer of gas molecules of real gas in equation (A1):

$$\theta = \frac{p/Z}{p_L + p/Z} \tag{A1}$$

where θ is gas coverage of real gas, dimensionless, p_L is Langmuir pressure (Pa), and Z is gas compressibility factor, dimensionless. When gas molecules are adsorbed on the pore surface, they reduce the pore space available to the remaining gas molecules for flow. Under the assumption of a homogenous loading of adsorbed gas molecules on the surface, the effective pore radius can be expressed as

$$r_{eff} = r - d_m\theta \tag{A2}$$

A2. Real Gas Effect on Gas Property

It has been recognised that the critical pressure P_c (Pa) and temperature T_c (K) of the gas are influenced by the pore space, when the pore diameter is below tens nanometers, as are the gas PVT and viscosity. In this

work, Islam's equations given in Islam et al. (2015b) are applied for critical temperature and pressure in nanopores, as shown in equations (A3) and (A4).

$$T_c = \frac{8}{27bR}\left[a - 2\sigma^3 \varepsilon N^2 \frac{\sigma}{r}\left(2.6275 - 0.6743\frac{\sigma}{r}\right)\right] \tag{A3}$$

$$P_c = \frac{8}{27b^2}\left[a - 2\sigma^3 \varepsilon N^2 \frac{\sigma}{r}\left(2.6275 - 0.6743\frac{\sigma}{r}\right)\right] \tag{A4}$$

where a is the vdW energy parameter (Padm^6 mol^{-2}), b is the vdW energy parameter (dm^3 mol^{-1}), σ is the Lennard-Jones size parameter (m), ε is Lennard-Jones energy parameter, dimensionless, and N is Avogadro number. It has been shown that the critical shifts of T_c and P_c expressed by equations (A3) and (A4) are in good agreement compared to the laboratory data and molecular simulation (Islam et al., 2015b).

By the same definitions of the pseudo reduced pressure and temperature, P_{pr} and T_{pr} as shown in equations (A5) and (A6), the modified van der Waals (vdW) Equation of State is developed in Mahmoud (2014) for the gas compressibility factor Z (equation (A7)) which is valid over a wide pressure range.

$$P_{pr} = \frac{P}{P_c} \tag{A5}$$

$$T_{pr} = \frac{T}{T_c} \tag{A6}$$

$$Z = (0.702e^{-2.5T_{pr}})P_{pr}^2 - 5.524e^{-2.5T_{pr}}P_{pr} + 0.044T_{pr}^2 - 0.164T_{pr} + 1.15 \tag{A7}$$

where P_{pr} is pseudo reduced pressure, dimensionless, and T_{pr} is pseudo reduced temperature, dimensionless. Lee et al. (1966) developed an empirical gas viscosity model for natural gases that has been used for the confined pores (Bui et al., 2016; Kim et al., 2016; Landry et al., 2016; Wang et al., 2017):

$$\mu = (1\times10^{-4})K\ \exp\left(X\rho^Y\right) \tag{A8}$$

$$\rho = 1.4935\times10^{-3}\frac{pM}{ZT} \tag{A9}$$

$$K = \frac{(9.379 + 0.01607M)T^{1.5}}{(209.2 + 19.26M + T)} \tag{A10}$$

$$X = 3.448 + \frac{986.4}{T} + 0.01009M \tag{A11}$$

$$Y = 2.447 - 0.2224X \tag{A12}$$

where ρ is gas density (kg/m^3) and M is gas molecular weight (g/mol).

A3. Free Gas Flow in the Full Flow Regimes

As mentioned above, the full range of gas flow regimes are identified by the Knudsen number, the ratio of the mean free path of gas molecules and the effective radius of a capillary with the presence of gas adsorption as given in equation (A2). It has been shown that the mean free path length for ideal gas and real gas differs due to their differences in gas PVT and viscosity (Villazon et al., 2011), where the mean free path λ (m) can be expressed by equation (A13) for real gas.

$$\lambda = \sqrt{\frac{\pi ZRT}{2M}}\frac{\mu}{p} \tag{A13}$$

The Knudsen number in organic pores can be written as

$$K_n = \frac{\lambda}{r_{eff}} \tag{A14}$$

In this work, a unified Hagen-Poiseuille-type equation developed by Beskok and Karniadakis (1999) is applied for modeling gas flow. For a capillary with a circular cross section, the volumetric gas flow q through is given as follows:

$$q = f(Kn)\frac{\pi R_h^4}{8\mu}\frac{\Delta p_h}{l} \tag{A15}$$

where R_h is the capillary radius (m), l is the length of the capillary (m), and Δp_h is the pressure drop on the capillary (Pa). The flow condition function $f(Kn)$ is given by

$$f(Kn) = (1+\alpha K_n)\left(1+\frac{4K_n}{1-\beta K_n}\right) \tag{A16}$$

The parameter α in equation (A16) is a dimensionless rarefaction coefficient, which can be written as

$$\alpha = \frac{128}{15\pi^2}\tan^{-1}\left[4.0{K_n}^{0.4}\right] \tag{A17}$$

Though the slip coefficient $\beta = -1$ initially can only be applied to a slip flow condition, evidence based on comparisons of the model with the DSMC and Boltzmann solutions (Karniadakis et al., 2006) showed that $\beta = -1$ is valid within the the full range of flow regimes.

According to equation (A15), free gas flow conductance can be written as

$$g_{free} = \frac{\pi r_{eff}^4 f(K_n)}{8\mu l} \tag{A18}$$

A4. Surface Diffusion of Adsorbed Gas

Surface diffusion of adsorbed gas molecules has long been considered as one of the key transport mechanisms in organic pores because of the large amount of adsorbed gas in organic shales. It can be modeled as the general diffusion process, using the molar flow rate per unit area of the concentration gradient within the adsorbed monolayer as developed in Cunningham and Williams (1980):

$$J_a = D_s\frac{dC_a}{dx} \tag{A19}$$

where J_a is the molar flow rate per unit area (mol/(m^2 s)), D_s is the surface diffusion coefficient (m^2/s), and C_a is adsorbed gas concentration (mol/m^3). C_a is calculated assuming Langmuir adsorption and is given by

$$C_a = C_{amax}\theta \tag{A20}$$

where C_{amax} is the maximum adsorbed gas concentration inside the nanoporous organic matter (mol/m^3) and C_{amax} can be expressed as (Wasaki & Akkutlu, 2015):

$$C_{amax} = \frac{C_{max}}{\varepsilon_{ks}} \tag{A21}$$

where C_{max} is the maximum adsorbed gas concentration inside the total core sample (mol/m^3) and ε_{ks} is the total organic grain volume per total grain volume, dimensionless. Combining equations (A19–A21), molar flow rate J_A (mol/s) in the adsorbed layer is then expressed below:

$$J_A = D_s C_{amax}\frac{d\theta}{dp}\pi\left(r^2 - r_{eff}^2\right)\frac{dp}{dx} \tag{A22}$$

From equation (A22), volumetric flow rate V_A (m^3/s) is

$$V_A = \frac{M}{\rho}D_s C_{amax}\frac{d\theta}{dp}\pi\left(r^2 - r_{eff}^2\right)\frac{dp}{dx} \tag{A23}$$

Based on Hwang and Kammermeyer's model (Hwang & Kammermeyer, 1966), combined with methane adsorption experimental data, the surface diffusion coefficient for methane D_{s0} (when gas coverage is zero, m^2/s) can be expressed as (Guo et al., 2008)

$$D_{s0} = 8.29\times10^{-7}T^{0.5}\exp\left(-\frac{\Delta H^{0.8}}{RT}\right) \tag{A24}$$

The isosteric adsorption heat ΔH is a function of gas coverage (Pan et al., 1998; Wang et al., 2012), according to Nodzeński (1998), the isosteric adsorption heat and gas coverage have a linear relationship and can be given as

$$\Delta H = \eta\theta + \Delta H(0) \tag{A25}$$

where $\Delta H(0)$ is the isosteric adsorption heat at zero gas coverage (J/mol) and η is the fitting coefficients of isosteric adsorption heat (J/mol). The surface diffusion coefficient in equation (A24) is obtained under a low pressure condition by theory and experiments and is a function of gas molecular weight, temperature, and gas activation energy, isosteric adsorption heat and independent of pressure (Hwang & Kammermeyer, 1966). In order to describe the gas surface diffusion in nanopores of shale gas reservoirs under a high pressure condition, the influence of gas coverage on surface diffusion is considered. Chen and Yang (1991) used the kinetic method to calculate the surface diffusion coefficient:

$$D_s = D_{s0}\frac{(1-\theta)+\frac{\kappa}{2}\theta(2-\theta)+\{H(1-\kappa)\}(1-\kappa)\frac{\kappa}{2}\theta^2}{\left(1-\theta+\frac{\kappa}{2}\theta\right)^2} \tag{A26}$$

$$H(1-\kappa)=0, \kappa \geq 1; 1, 0 \leq \kappa \leq 1 \tag{A27}$$

$$\kappa = \frac{\kappa_b}{\kappa_m} \tag{A28}$$

where κ_b is rate constant for blockage in surface diffusion, κ_m is rate constant for forward migration in surface diffusion, κ is ratio of the rate constant for blockage to the rate constant for forward migration, and $H(1 - \kappa)$ is Heaviside function, dimensionless. When $\kappa_m > \kappa_b$, surface diffusion occurs. When $\kappa_m < \kappa_b$, gas molecules are blocked and surface diffusion stops. According to equation (A23), adsorbed gas flow conductance can be written as

$$g_{surface} = \frac{1}{l}\frac{M}{\rho}D_s C_{a\max}\frac{d\theta}{dp}\pi\left(r^2 - r_{eff}^2\right) \tag{A29}$$

A5. Gas Flow Conductance for a Cylindrical Capillary in Organic Pores

For a cylindrical capillary representing an organic pore, gas flow conductance can be derived by combining the contributions of free gas, and surface diffusion of adsorbed gas, taking into consideration the reduction of the pore space due to adsorbed gas and the effect of confined pore space on gas PVT and viscosity:

$$g_{or} = \frac{\pi r_{eff}^4}{8\mu l}\left(1+\frac{128}{15\pi^2}\tan^{-1}[4.0{K_n}^{0.4}]K_n\right)\left(1+\frac{4K_n}{1+K_n}\right)+\frac{1}{l}\frac{M}{\rho}D_s C_{a\max}\frac{d\theta}{dp}\pi\left(r^2 - r_{eff}^2\right) \tag{A30}$$

For such a capillary of a given pore radius its apparent permeability is defined as follows:

$$k_{or} = \frac{g_{or}\mu l}{\pi r^2} \tag{A31}$$

Appendix B: Absolute Gas Permeability at Different Temperatures and Pressures

Absolute gas permeability at different temperatures and pressures is shown in Table B1.

Table B1
Absolute Gas Permeability at Different Temperatures and Pressures

k_{abs_gas} (μm^2)	T (K) (P = 40 MPa)	k_{abs_gas} (μm^2)	P (MPa) (T = 400 K)
1.9036×10^{-6}	350	2.0519×10^{-6}	5
1.9075×10^{-6}	400	1.9917×10^{-6}	10
1.9126×10^{-6}	450	1.9394×10^{-6}	20
1.9191×10^{-6}	500	1.9181×10^{-6}	30
1.9269×10^{-6}	550	1.9075×10^{-6}	40
1.9362×10^{-6}	600	1.9015×10^{-6}	50

Acknowledgments
This project is supported by the National Natural Science Foundation of China (51674280, 51504276, 51234007, 51711530131, and 51490654), Shandong Provincial Natural Science Foundation, China (ZR2014EEP018), CNOOC Science Project: Research on overseas shale oil and gas productivity evaluation method (YXKY-2016-ZY-03), the Major Projects of the National Science and Technology (2016ZX05061), the Fundamental Research Funds for the Central Universities (No. 17CX05003, 18CX06008A, 17CX02008A), Applied basic research projects of Qingdao innovation plan (16-5-1-38-jch) and the Graduate School Innovation Program of China University of Petroleum (YCX2017019). The data used are listed in the figures and tables in this paper.

References

Afsharpoor, A., & Javadpour, F. (2016). Liquid slip flow in a network of shale noncircular nanopores. *Fuel*, *180*, 580–590.
Afsharpoor, A., Javadpour, F., Wu, J., Ko, L. T., & Liang, Q. (2017). Network modeling of liquid flow in Yanchang shale. *Interpretation*, *5*(2), SF99–SF107.
Akkutlu, I. Y., & Didar, B. R. (2013). Pore-size dependence of fluid phase behavior and properties in organic-rich shale reservoirs. In *SPE international symposium on oilfield chemistry*. Richardson, TX: Society of Petroleum Engineers.
Al-Shemmeri, T. (2012). *Engineering fluid mechanics*. London, UK: Bookboon.
Arns, J.-Y., Arns, C. H., Sheppard, A. P., Sok, R. M., Knackstedt, M. A., & Pinczewski, W. V. (2003). Relative permeability from tomographic images; effect of correlated heterogeneity. *Journal of Petroleum Science and Engineering*, *39*(3), 247–259.
Arns, J.-Y., Robins, V., Sheppard, A. P., Sok, R. M., Pinczewski, W. V., & Knackstedt, M. A. (2004). Effect of network topology on relative permeability. *Transport in Porous Media*, *55*(1), 21–46.
Barrat, J.-L., & Bocquet, L. (1999). Large slip effect at a nonwetting fluid-solid interface. *Physical Review Letters*, *82*(23), 4671.
Belyaev, A. V., & Vinogradova, O. I. (2010). Effective slip in pressure-driven flow past super-hydrophobic stripes. *Journal of Fluid Mechanics*, *652*, 489–499.
Berg, S., Cense, A. W., Hofman, J. P., & Smits, R. M. M. (2007). *Flow in porous media with slip boundary condition*. Paper presented at the Society of Core Analysts SCA2007-13, Calgary, Canada.
Beskok, A., & Karniadakis, G. E. (1999). Report: A model for flows in channels, pipes, and ducts at micro and nano scales. *Microscale Thermophysical Engineering*, *3*(1), 43–77.
Blunt, M. J., Bijeljic, B., Dong, H., Gharbi, O., Iglauer, S., Mostaghimi, P., et al. (2013). Pore-scale imaging and modelling. *Advances in Water Resources*, *51*, 197–216.
Blunt, M. J., Jackson, M. D., Piri, M., & Valvatne, P. H. (2002). Detailed physics, predictive capabilities and macroscopic consequences for pore-network models of multiphase flow. *Advances in Water Resources*, *25*(8), 1069–1089.
Bui, B. T., Liu, H.-H., Chen, J., & Tutuncu, A. N. (2016). Effect of capillary condensation on gas transport in shale: A pore-scale model study. *SPE Journal*, *21*(2). https://doi.org/10.2118/179731-PA
Campbell, S. E., Luengo, G., Srdanov, V., & Israelachvili, J. N. (1996). Very low viscosity at the solid-liquid interface induced by adsorbed C60 monolayers. *Nature*, *382*(6591), 520.
Chalmers, G. R., Bustin, R. M., & Power, I. M. (2012). Characterization of gas shale pore systems by porosimetry, pycnometry, surface area, and field emission scanning electron microscopy/transmission electron microscopy image analyses: Examples from the Barnett, Woodford, Haynesville, Marcellus, and Doig units. *American Association of Petroleum Geologists Bulletin*, *96*(6), 1099–1119.
Chandler, R., Koplik, J., Lerman, K., & Willemsen, J. F. (1982). Capillary displacement and percolation in porous media. *Journal of Fluid Mechanics*, *119*, 249–267.
Charoensuppanimit, P., Mohammad, S. A., & Gasem, K. A. M. (2016). Measurements and modeling of gas adsorption on shales. *Energy & Fuels*, *30*(3), 2309–2319.
Chen, L., Kang, Q., Dai, Z., Viswanathan, H. S., & Tao, W. (2015b). Permeability prediction of shale matrix reconstructed using the elementary building block model. *Fuel*, *160*, 346–356.
Chen, L., Kang, Q., Pawar, R., He, Y.-L., & Tao, W.-Q. (2015c). Pore-scale prediction of transport properties in reconstructed nanostructures of organic matter in shales. *Fuel*, *158*, 650–658.
Chen, L., Zhang, L., Kang, Q., Viswanathan, H. S., Yao, J., & Tao, W. (2015a). Nanoscale simulation of shale transport properties using the lattice Boltzmann method: Permeability and diffusivity. *Scientific Reports*, *5*, 8089.
Chen, Y. D., & Yang, R. T. (1991). Concentration dependence of surface diffusion and zeolitic diffusion. *AIChE Journal*, *37*(10), 1579–1582.
Civan, F. (2010). Effective correlation of apparent gas permeability in tight porous media. *Transport in Porous Media*, *82*(2), 375–384.
Civan, F., Devegowda, D., & Sigal, R. F. (2013). Critical evaluation and improvement of methods for determination of matrix permeability of shale. In *SPE annual technical conference and exhibition*. Richardson, TX: Society of Petroleum Engineers.
Civan, F., Rai, C. S., & Sondergeld, C. H. (2011). Shale-gas permeability and diffusivity inferred by improved formulation of relevant retention and transport mechanisms, *Transport in Porous Media*, *86*(3), 925–944.
Cottin-Bizonne, C., Barrat, J.-L., Bocquet, L., & Charlaix, E. (2003). Low-friction flows of liquid at nanopatterned interfaces. *Nature Materials*, *2*(4), 237–240.
Cunningham, R. E., & Williams, R. J. J. (1980). *Diffusion in gases and porous media*. Berlin, Germany: Springer.
Darabi, H., Ettehad, A., Javadpour, F., & Sepehrnoori, K. (2012). Gas flow in ultra-tight shale strata. *Journal of Fluid Mechanics*, *710*, 641–658.
Devegowda, D., Sapmanee, K., Civan, F., & Sigal, R. F. (2012). Phase behavior of gas condensates in shales due to pore proximity effects: Implications for transport, reserves and well productivity. In *SPE annual technical conference and exhibition*. Richardson, TX: Society of Petroleum Engineers.
Dewers, T. A., Heath, J., Ewy, R., & Duranti, L. (2012). Three-dimensional pore networks and transport properties of a shale gas formation determined from focused ion beam serial imaging. *International Journal of Oil, Gas and Coal Technology*, *5*(2–3), 229–248.
Dong, H., & Blunt, M. J. (2009). Pore-network extraction from micro-computerized-tomography images. *Physical Review E*, *80*(3), 36307.
Gao, J., Szoszkiewicz, R., Landman, U., & Riedo, E. (2007). Structured and viscous water in subnanometer gaps. *Physical Review B*, *75*(11), 115415.
Ghanbarian, B., & Javadpour, F. (2017). Upscaling pore pressure-dependent gas permeability in shales. *Journal of Geophysical Research: Solid Earth*, *122*, 2541–2552. https://doi.org/10.1002/2016JB013846
Goertz, M. P., Houston, J. E., & Zhu, X.-Y. (2007). Hydrophilicity and the viscosity of interfacial water. *Langmuir*, *23*(10), 5491–5497.
Granick, S., Zhu, Y., & Lee, H. (2003). Slippery questions about complex fluids flowing past solids. *Nature Materials*, *2*(4), 221–227.
Guo, L., Peng, X., & Wu, Z. (2008). Dynamical characteristics of methane adsorption on monolith nanometer activated carbon. *Journal of Chemical Industry and Engineering*, *11*, 7.
Heller, R., & Zoback, M. (2014). Adsorption of methane and carbon dioxide on gas shale and pure mineral samples. *Journal of Unconventional Oil and Gas Resources*, *8*, 14–24.
Hoang, H., & Galliero, G. (2012). Local viscosity of a fluid confined in a narrow pore. *Physical Review E*, *86*(2), 21202.
Holt, J. K., Park, H. G., Wang, Y., Stadermann, M., Artyukhin, A. B., Grigoropoulos, C. P., et al. (2006). Fast mass transport through sub-2-nanometer carbon nanotubes. *Science*, *312*(5776), 1034–1037.
Hoogland, F., Lehmann, P., Mokso, R., & Or, D. (2016b). Drainage mechanisms in porous media: From piston-like invasion to formation of corner flow networks. *Water Resources Research*, *52*, 8413–8436. https://doi.org/10.1002/2016WR019299
Hoogland, F., Lehmann, P., & Or, D. (2016a). Drainage dynamics controlled by corner flow: Application of the foam drainage equation. *Water Resources Research*, *52*, 8402–8412. https://doi.org/10.1002/2016WR019477

Huang, X., Bandilla, K. W., & Celia, M. A. (2016). Multi-physics pore-network modeling of two-phase shale matrix flows. *Transport in Porous Media*, *111*(1), 123–141.
Hwang, S., & Kammermeyer, K. (1966). Surface diffusion in microporous media. *The Canadian Journal of Chemical Engineering*, *44*(2), 82–89.
Islam, A. W., Patzek, T. W., & Sun, A. Y. (2015a). Thermodynamics phase changes of nanopore fluids. *Journal of Natural Gas Science and Engineering*, *25*, 134–139. https://doi.org/10.1016/j.jngse.2015.04.035
Jassim, F. A., & Altaani, F. H. (2013). Hybridization of OTSU method and median filter for color image segmentation. *International Journal of Soft Computing and Engineering*, *3*(2).
Javadpour, F. (2009). Nanopores and apparent permeability of gas flow in mudrocks (shales and siltstone). *Journal of Canadian Petroleum Technology*, *48*(8), 16–21.
Javadpour, F., Fisher, D., & Unsworth, M. (2007). Nanoscale gas flow in shale gas sediments. *Journal of Canadian Petroleum Technology*, *46*(10).
Javadpour, F., McClure, M., & Naraghi, M. E. (2015). Slip-corrected liquid permeability and its effect on hydraulic fracturing and fluid loss in shale. *Fuel*, *160*, 549–559.
Joekar-Niasar, V., Prodanović, M., Wildenschild, D., & Hassanizadeh, S. M. (2010). Network model investigation of interfacial area, capillary pressure and saturation relationships in granular porous media. *Water Resources Research*, *46*, W06526. https://doi.org/10.1029/2009WR008585
Karniadakis, G. E., Beskok, A., & Aluru, N. (2006). *Microflows and nanoflows: Fundamentals and simulation*. Berlin, Germany: Springer Science & Business Media.
Kim, C., Jang, H., Lee, Y., & Lee, J. (2016). Diffusion characteristics of nanoscale gas flow in shale matrix from Haenam basin, Korea. *Environmental Earth Sciences*, *75*(4), 350. https://doi.org/10.1007/s12665-016-5267-4
Kloubek, J. (1981). Hysteresis in porosimetry. *Powder Technology*, *29*(1), 63–73.
Korb, J.-P., Nicot, B., Louis-Joseph, A., Bubici, S., & Ferrante, G. (2014). Dynamics and wettability of oil and water in oil shales. *Journal of Physical Chemistry C*, *118*(40), 23212–23218.
Lan, Q., Xu, M., Binazadeh, M., Dehghanpour, H., & Wood, J. M. (2015). A comparative investigation of shale wettability: The significance of pore connectivity. *Journal of Natural Gas Science and Engineering*, *27*, 1174–1188.
Landry, C. J., Prodanović, M., & Eichhubl, P. (2016). Direct simulation of supercritical gas flow in complex nanoporous media and prediction of apparent permeability. *International Journal of Coal Geology*, *159*, 120–134.
Lauga, E., & Stone, H. A. (2003). Effective slip in pressure-driven Stokes flow. *Journal of Fluid Mechanics*, *489*, 55.
Lee, A. L., Gonzalez, M. H., & Eakin, B. E. (1966). The viscosity of natural gases. *Journal of Petroleum Technology*, *18*(8), 991–997.
Lee, T., Bocquet, L., & Coasne, B. (2016). Activated desorption at heterogeneous interfaces and long-time kinetics of hydrocarbon recovery from nanoporous media. *Nature Communications*, *7*, 11890.
Li, J., Li, X., Wu, K., Feng, D., Zhang, T., & Zhang, Y. (2017). Thickness and stability of water film confined inside nanoslits and nanocapillaries of shale and clay. *International Journal of Coal Geology*, *179*, 253–268.
Li, J., Li, X., Wu, K., Wang, X., Shi, J., Yang, L., et al. (2016). Water sorption and distribution characteristics in clay and shale: Effect of surface force. *Energy & Fuels*, *30*(11), 8863–8874.
Lindquist, W. B., Venkatarangan, A., Dunsmuir, J., & Wong, T. (2000). Pore and throat size distributions measured from synchrotron X-ray tomographic images of Fontainebleau sandstones. *Journal of Geophysical Research*, *105*(B9), 21509–21527.
Liu, Y., Wang, Q., Zhang, L., & Wu, T. (2005). Dynamics and density profile of water in nanotubes as one-dimensional fluid. *Langmuir*, *21*(25), 12025–12030.
Loyalka, S. K., & Hamoodi, S. A. (1990). Poiseuille flow of a rarefied gas in a cylindrical tube: Solution of linearized Boltzmann equation. *Physics of Fluids A Fluid Dynamics*, *2*(11), 2061–2065.
Lu, H. M., & Jiang, Q. (2005). Size-dependent surface tension and Tolman's length of droplets. *Langmuir*, *21*(2), 779–781.
Ma, J., & Couples, G. D. (2015). *Assessing impact of shale gas adsorption on free-gas permeability via a pore network flow model*. Paper presented at the Unconventional Resources Technology Conference (URTEC).
Ma, J., Sanchez, J. P., Wu, K., Couples, G. D., & Jiang, Z. (2014a). A pore network model for simulating non-ideal gas flow in micro-and nano-porous materials. *Fuel*, *116*, 498–508.
Ma, J., Zhang, X., Jiang, Z., Ostadi, H., Jiang, K., & Chen, R. (2014b). Flow properties of an intact MPL from nano-tomography and pore network modelling. *Fuel*, *136*, 307–315.
Mahmoud, M. (2014). Development of a new correlation of gas compressibility factor (Z-factor) for high pressure gas reservoirs. *Journal of Energy Resources Technology*, *136*(1), 12903.
Majumder, M., Chopra, N., Andrews, R., & Hinds, B. J. (2005). Nanoscale hydrodynamics: Enhanced flow in carbon nanotubes. *Nature*, *438*(7064), 44.
Mashl, R. J., Joseph, S., Aluru, N. R., & Jakobsson, E. (2003). Anomalously immobilized water: A new water phase induced by confinement in nanotubes. *Nano Letters*, *3*(5), 589–592.
Mehmani, A., Prodanović, M., & Javadpour, F. (2013). Multiscale, multiphysics network modeling of shale matrix gas flows. *Transport in Porous Media*, *99*(2), 377–390.
Neek-Amal, M., Peeters, F. M., Grigorieva, I. V., & Geim, A. K. (2016). Commensurability effects in viscosity of nanoconfined water. *ACS Nano*, *10*(3), 3685–3692.
Nelson, P. H. (2009). Pore-throat sizes in sandstones, tight sandstones, and shales. *American Association of Petroleum Geologists Bulletin*, *93*(3), 329–340.
Neto, C., Evans, D. R., Bonaccurso, E., Butt, H.-J., & Craig, V. S. J. (2005). Boundary slip in Newtonian liquids: A review of experimental studies. *Reports on Progress in Physics*, *68*(12), 2859.
Nodzeński, A. (1998). Sorption and desorption of gases (CH_4, CO_2) on hard coal and active carbon at elevated pressures. *Fuel*, *77*(11), 1243–1246.
Odusina, E. O., Sondergeld, C. H., & Rai, C. S. (2011). NMR study of shale wettability. In *Canadian unconventional resources conference*. Richardson, TX: Society of Petroleum Engineers.
Okabe, H., & Blunt, M. J. (2005). Pore space reconstruction using multiple-point statistics. *Journal of Petroleum Science and Engineering*, *46*(1), 121–137.
Oren, P.-E., Bakke, S., & Arntzen, O. J. (1998). Extending predictive capabilities to network models. *SPE Journal*, *3*(4), 324–336.
Ortiz-Young, D., Chiu, H.-C., Kim, S., Voïtchovsky, K., & Riedo, E. (2013). The interplay between apparent viscosity and wettability in nanoconfined water. *Nature Communications*, *4*, 2482.
Pan, H., Ritter, J. A., & Balbuena, P. B. (1998). Isosteric heats of adsorption on carbon predicted by density functional theory. *Industrial & Engineering Chemistry Research*, *37*(3), 1159–1166.

Raviv, U., Laurat, P., & Klein, J. (2001). Fluidity of water confined to subnanometre films. *Nature*, *413*(6851), 51–54.
Ryazanov, A. V., Van Dijke, M. I. J., & Sorbie, K. S. (2009). Two-phase pore-network modelling: Existence of oil layers during water invasion. *Transport in Porous Media*, *80*(1), 79–99.
Singh, H. (2013). *Nonempirical apparent permeability of shale*. Paper presented at the Unconventional Resources Technology Conference (URTEC).
Singh, H., & Javadpour, F. (2016). Langmuir slip-Langmuir sorption permeability model of shale. *Fuel*, *164*, 28–37.
Song, W., Yao, J., Li, Y., Sun, H., Zhang, L., Yang, Y., et al. (2016a). Apparent gas permeability in an organic-rich shale reservoir. *Fuel*, *181*, 973–984.
Song, W., Yao, J., Li, Y., Yang, Y., & Sun, H. (2016b). New pore size distribution calculation model based on chord length and digital image. *Journal of Natural Gas Science and Engineering*, *48*, 111–118.
Song, W., Yao, J., Ma, J., Couples, G., & Li, Y. (2017). Assessing relative contributions of transport mechanisms and real gas properties to gas flow in nanoscale organic pores in shales by pore network modelling. *International Journal of Heat and Mass Transfer*, *113*, 524–537.
Suhrer, M., Toelke, J., Diaz, E., Grader, A., Walls, J., Restrepo, D. P., et al. (2013). *Computed two-phase relative permeability using digital rock physics in a shale formation*. Paper presented at the Society of Core Analysts SCA2013-037.
Sun, H., Yao, J., Fan, D., Wang, C., & Sun, Z. (2015). Gas transport mode criteria in ultra-tight porous media. *International Journal of Heat and Mass Transfer*, *83*, 192–199.
Tang, X., Ripepi, N., Stadie, N. P., Yu, L., & Hall, M. R. (2016). A dual-site Langmuir equation for accurate estimation of high pressure deep shale gas resources. *Fuel*, *185*, 10–17.
Thomas, J. A., & McGaughey, A. J. H. (2008). Reassessing fast water transport through carbon nanotubes. *Nano Letters*, *8*(9), 2788–2793.
Valvatne, P. H. (2004). *Predictive pore-scale modelling of multiphase flow*. London, UK: Imperial College London.
Valvatne, P. H., & Blunt, M. J. (2004). Predictive pore-scale modeling of two-phase flow in mixed wet media. *Water Resources Research*, *40*, W07406. https://doi.org/10.1029/2003WR002627
Vega, C., & De Miguel, E. (2007). Surface tension of the most popular models of water by using the test-area simulation method. *Journal of Chemical Physics*, *126*(15), 154707.
Villazon, M., German, G., Sigal, R. F., Civan, F., & Devegowda, D. (2011). Parametric investigation of shale gas production considering nano-scale pore size distribution, formation factor, and non-Darcy flow mechanisms. In *SPE annual technical conference and exhibition*. Richardson, TX: Society of Petroleum Engineers.
Vinogradova, O. I. (1995). Drainage of a thin liquid film confined between hydrophobic surfaces. *Langmuir*, *11*(6), 2213–2220.
Vinogradova, O. I. (1999). Slippage of water over hydrophobic surfaces. *International Journal of Mineral Processing*, *56*(1), 31–60.
Walls, J. D., & Sinclair, S. W. (2011). Eagle Ford shale reservoir properties from digital rock physics. *First Break*, *29*(6), 97–101.
Wang, J., Luo, H., Liu, H., Cao, F., Li, Z., & Sepehrnoori, K. (2017), An integrative model to simulate gas transport and production coupled with gas adsorption, non-Darcy flow, surface diffusion, and stress dependence in organic-shale reservoirs. *SPE Journal*, *22*(1). https://doi.org/10.2118/174996-PA
Wang, Y., Ercan, C., Khawajah, A., & Othman, R. (2012). Experimental and theoretical study of methane adsorption on granular activated carbons. *AIChE Journal*, *58*(3), 782–788.
Wang, Y., Zhu, Y., Liu, S., & Zhang, R. (2016). Methane adsorption measurements and modeling for organic-rich marine shale samples. *Fuel*, *172*, 301–309.
Wasaki, A., & Akkutlu, I. Y. (2015). Permeability of organic-rich shale. *SPE Journal*, *20*(6).
Whitby, M., Cagnon, L., Thanou, M., & Quirke, N. (2008). Enhanced fluid flow through nanoscale carbon pipes. *Nano Letters*, *8*(9), 2632–2637.
Wilkinson, D., & Willemsen, J. F. (1983). Invasion percolation: A new form of percolation theory. *Journal of Physics A: Mathematical and General*, *16*(14), 3365.
Wu, K., Chen, Z., Li, J., Li, X., Xu, J., & Dong, X. (2017). Wettability effect on nanoconfined water flow. *Proceedings of the National Academy of Sciences of the United States of America*, *114*(13), 3358–3363.
Wu, K., Chen, Z., Li, X., Guo, C., & Wei, M. (2016). A model for multiple transport mechanisms through nanopores of shale gas reservoirs with real gas effect–adsorption-mechanic coupling. *International Journal of Heat and Mass Transfer*, *93*, 408–426.
Wu, K., Li, X., Wang, C., Yu, W., & Chen, Z. (2014). *Apparent permeability for gas flow in shale reservoirs coupling effects of gas diffusion and desorption*. Paper presented at the Proceedings of the 2nd Unconventional Resources Technology Conference (pp. 1–18). https://doi.org/10.15530/urtec-2014-1921039
Wu, K., Li, X., Wang, C., Yu, W., & Chen, Z. (2015). Model for surface diffusion of adsorbed gas in nanopores of shale gas reservoirs. *Industrial & Engineering Chemistry Research*, *54*(12), 3225–3236.
Wu, T., Li, X., Zhao, J., & Zhang, D. (2017), Multiscale pore structure and its effect on gas transport in organic-rich shale. *Water Resources Research*, *53*, 5438–5450. https://doi.org/10.1002/2017WR020780
Xiong, X., Devegowda, D., Villazon, M., German, G., Sigal, R. F., & Civan, F. (2012). A fully-coupled free and adsorptive phase transport model for shale gas reservoirs including non-Darcy flow effects. In *SPE annual technical conference and exhibition*. Richardson, TX: Society of Petroleum Engineers.
Xu, M., & Dehghanpour, H. (2014). Advances in understanding wettability of gas shales. *Energy & Fuels*, *28*(7), 4362–4375.
Yang, Y., Yao, J., Wang, C., Gao, Y., Zhang, Q., An, S., et al. (2015). New pore space characterization method of shale matrix formation by considering organic and inorganic pores. *Journal of Natural Gas Science and Engineering*, *27*, 496–503.
Yi, Z., Lin, M., Jiang, W., Zhang, Z., Li, H., & Gao, J. (2017), Pore network extraction from pore space images of various porous media systems. *Water Resources Research*, *53*, 3424–3445. https://doi.org/10.1002/2016WR019272
Yu, W., Sepehrnoori, K., & Patzek, T. W. (2016). Modeling gas adsorption in Marcellus Shale with Langmuir and BET isotherms. *SPE Journal*, *21*(2).
Zhang, P., Hu, L., Meegoda, J. N., & Gao, S. (2015). Micro/nano-pore network analysis of gas flow in shale matrix. *Scientific Reports*, *5*, 13501.